




## Article

# Characterisation of fibrous ferrierite in the rhyolitic tuffs at Lovelock, Nevada, USA

Alessandro Zoboli<sup>1</sup>, Dario Di Giuseppe<sup>1\*</sup> , Cecilia Baraldi<sup>2</sup>, Maria Cristina Gamberini<sup>2</sup>, Daniele Malferrari<sup>1</sup>, Giancarlo Urso<sup>3</sup>, Magdalena Lassinantti Gualtieri<sup>4</sup>, Mark Bailey<sup>5</sup> and Alessandro F. Gualtieri<sup>1</sup>

<sup>1</sup>Department of Chemical and Geological Sciences, University of Modena and Reggio Emilia, Via Campi 103, Modena, I-41125, Italy; <sup>2</sup>Department of Life Sciences, University of Modena and Reggio Emilia, via Campi 103, Modena, I-41125, Italy; <sup>3</sup>Centro Interdipartimentale Grandi Strumenti, CIGS, University of Modena and Reggio Emilia, via Campi 185, Modena, I-41125, Italy; <sup>4</sup>Department of Engineering “Enzo Ferrari”, University of Modena and Reggio Emilia, I-41125, Modena, Italy; and <sup>5</sup>Asbestos TEM Laboratories, 600 Bancroft Way, Suite A, Berkeley, California, 94710, USA.

### Abstract

Ferrierite is the name for a series of zeolite-group of minerals which includes three species with the same ferrierite framework (FER) crystal structure but different extra-framework cations. Recent studies have shown that ferrierite can exhibit a fibrous-asbestiform crystal habit and may possess the same properties as carcinogenic fibrous erionite. Characterisation of the ferrierite in and around a mine location will be helpful in assessing the potential for toxic outcomes of exposure in the mine and any local population.

The zeolite-rich tuff deposit of Lovelock, Nevada, USA is the largest occurrence of diagenetic ferrierite-Mg. A previous survey reported that ferrierite hosted in these rocks displays a fibrous morphology. However, these observations concerned a limited number of samples and until now there has been little evidence of widespread occurrence of fibrous ferrierite in the Lovelock deposit.

The main goal of this study was to perform a mineralogical and morphometric characterisation of the tuff deposit at Lovelock and evaluate the distribution of fibrous ferrierite in the outcrop. For this purpose, a multi-analytical approach including powder X-ray diffraction, scanning and transmission microscopies, micro-Raman spectroscopy, thermal analyses, and surface-area determination was applied.

The results prove fibrous ferrierite is widespread and intermixed with mordenite and orthoclase, although there are variations in the spatial distribution in the bedrock. The crystal habit of the ferrierite ranges from prismatic to asbestiform (elongated, thin and slightly flexible) and fibres are aggregated in bundles. According to the WHO counting criteria, most of the ferrierite fibres can be classified as breathable. While waiting for confirmatory *in vitro* and *in vivo* tests to assess the actual toxicity/pathogenicity potential of this mineral fibre, it is recommended to adopt a precautionary approach for mining operations in this area to reduce the risk of exposure.

**Keywords:** mineral fibres, rhyolitic tuffs, zeolite, ferrierite, health hazard

(Received 10 January 2019; accepted 20 March 2019; Accepted Manuscript online 22 April 2019; Associate Editor: Giancarlo Della Ventura)

### Introduction

Ferrierite is the name for a series of high-silica zeolite-group minerals which includes species with the same crystal structure (i.e. ferrierite framework, FER) but different extra-framework cations (Mg, K and Na). The structural framework belongs to the mordenite group (Gottardi and Galli, 1985). The name ‘ferrierite’ was given by Graham (1918) to honour Walter F. Ferrier, who first found the mineral on the north shore of Kamloops Lake, British Columbia, Canada. The first structure refinements of this zeolite series were conducted by Vaughan (1966) and Gramlich-Meier *et al.* (1984). The FER framework consists of ten-membered ring channels parallel to [001], intersected by eight-membered ring channels parallel to [010]. Six-membered ring channels also run along [001], and the intersection of the six-membered ring channels with the eight-

membered ring channels leads to the formation of the ‘ferrierite cavity’, a cage accessible through eight-membered ring windows (Arletti *et al.*, 2018; Gualtieri *et al.*, 2018a; Vaughan, 1966). Ferrierite, with general chemical formula  $(\text{Mg}_{0.5}\text{Na,K})_6[\text{Al}_6\text{Si}_{30}\text{O}_{72}]\cdot 20\text{H}_2\text{O}$  (Passaglia and Sheppard, 2001), commonly crystallises in the orthorhombic space group *Immm* (Vaughan, 1966; Gramlich-Meier *et al.*, 1984). However, Gramlich-Meier *et al.* (1985) refined the structure of ferrierite-Na (Mg-poor) in space group *P2<sub>1</sub>/n* with symmetry that apparently depends on both extra-framework and framework occupation.

Ferrierite has both a hydrothermal and diagenetic origin and is found mainly in the voids of volcanic rocks or in tuffaceous sediments (Arletti *et al.*, 2018; Gualtieri *et al.*, 2018a; Passaglia and Sheppard, 2001; Rice *et al.*, 1992). In both occurrences, ferrierite coexists with other high-silica zeolites (commonly mordenite and clinoptilolite), as well as carbonates, baryte, apatite, pyrite, cinnabar, chalcedony, feldspar and quartz (Gualtieri *et al.*, 2018a; Passaglia and Sheppard, 2001).

Ferrierite may exhibit different crystal habits: lath-like/lamellar, prismatic, needle-like, acicular, fibrous and asbestiform (Gualtieri *et al.* 2018a). A recent study by Gualtieri *et al.* (2018a) pointed out that fibrous ferrierite has the same chemical-physical

\*Author for correspondence: Dario Di Giuseppe, Email: [dario.digiuseppe@unimore.it](mailto:dario.digiuseppe@unimore.it)  
Cite this article: Zoboli A., Di Giuseppe D., Baraldi C., Gamberini M.C., Malferrari D., Urso G., Lassinantti Gualtieri M., Bailey M. and Gualtieri A.F. (2019) Characterisation of fibrous ferrierite in the rhyolitic tuffs at Lovelock, Nevada, USA. *Mineralogical Magazine* 83, 577–586. <https://doi.org/10.1180/mgm.2019.25>

properties (morphometric parameters, specific surface area and iron content) that are suspected to prompt adverse effects *in vivo* by fibrous erionite. Up to now, fibrous erionite is the only zeolite classified as a carcinogen for humans by the International Agency for Research on Cancer (IARC, 2012; 2017). As provided by long-term epidemiological studies and several animal carcinogenicity tests, fibrous erionite is responsible for epidemics of mesothelioma in Cappadocia, Turkey, where villages were built with erionite-bearing rocks (Carbone *et al.*, 2007; IARC, 2017). Because fibrous ferrierite may represent a potential health hazard, the acquisition of further information about its natural occurrence is essential to avoid potential exposure of workers handling this material (e.g. minimise dust generated by excavation activities) or populations living nearby fibrous ferrierite-rich outcrops (environmental exposure).

The tuff outcrop of Lovelock, in Pershing County, Nevada, USA, has the best known occurrence of diagenetic ferrierite (Rice *et al.*, 1992). This deposit was discovered in 1965 by E. Galli and is mainly composed of zeolitised rhyolitic pyroclastic rocks in which the zeolite content (ferrierite, mordenite and clinoptilolite) is >50 wt.% (Gualtieri *et al.*, 2018a). Investigations by Rice *et al.* (1992) on selected samples from cores drilled through the Lovelock deposit, have shown that ferrierite hosted in those rocks displays a fibrous morphology. The presence of fibrous ferrierite in this area was also reported by Gualtieri *et al.* (2018a). However, as previous studies concerned a limited number of samples, there is little evidence of the lateral continuity of the fibrous ferrierite in the Lovelock deposit.

This work has been conducted with the aim to: (1) assess if the occurrence of fibrous ferrierite described by Rice *et al.* (1992) is a singularity or widespread in the Lovelock deposit; (2) acquire new data on the mineralogy of the Lovelock deposit, with the analysis of a number of samples to improve previous knowledge on this site; (3) perform a crystal-chemical and morphological characterisation of the mineral fibres associated with the samples; and (4) evaluate, on the basis of the morphometric parameters length ( $L$ ) and diameter ( $D$ ), if these mineral fibres represent a potential hazard, according to the existing regulatory classification. To this aim, regulated fibres are classified according to the counting criteria of the World Health Organization:  $L \geq 5\mu\text{m}$ ,  $D \leq 3\mu\text{m}$  and  $L/D \geq 3:1$  (WHO, 1997).

## Geological overview

The Lovelock deposit occurs in a group of volcanic and sedimentary rocks of Tertiary age within the Trinity Range, Pershing County, northwest Nevada (Fig. 1) (Gualtieri *et al.*, 2018a). The study area is characterised by a sequence of welded ash flow tuffs and alluvial/lacustrine sedimentary deposits, yellowish to cream coloured, sitting on the Triassic metasediments (Crafford, 2007). Following the scheme proposed by Stewart and Carlson (1978) and Crafford (2007), Miocene–Pliocene rocks in Nevada are subdivided in three age groups, from the youngest to the oldest: T3 (6–17 Ma); T2 (18–34 Ma); and T1 (35–43 Ma). In addition, there are five primary compositional and (or) textural groupings: sedimentary (Ts3, Ts2 and TKs1); basaltic (Tb3 and Tb2); andesitic (Ta3, Ta2 and Ta1); tuffaceous (Tt3, Tt2 and Tt1); and rhyolitic (Tr3, Tr2 and Tr1). Ferrierite is hosted in diagenetically altered rhyolitic tuffaceous rocks (Tt3), together with mordenite, clinoptilolite, smectite, orthoclase and cristobalite. As illustrated in Fig. 1, the Lovelock deposit is characterised by both ferrierite-rich tuffs and mordenite-rich tuffs.

Diagenetic processes that allowed the crystallisation of zeolites occurred through the hydration reactions of the glassy fraction of pyroclastic sediments (Rice *et al.*, 1992). During diagenesis, the first phase crystallised in the sequence was smectite followed by ferrierite (the first zeolite to crystallise) together with K-feldspar. Clinoptilolite and mordenite crystallised later. Mordenite replaced clinoptilolite, whereas cristobalite crystallised together with clinoptilolite after ferrierite and orthoclase (Rice *et al.*, 1992).

According to Gualtieri *et al.* (2018a), the general chemical formula of the Lovelock ferrierite, as determined from EMPA analyses is:  $\text{Fe}_{0.16}^{3+}(\text{K}_{1.21}\text{Mg}_{2.11}\text{Ca}_{0.43}\text{Na}_{0.27})_{4.02}[\text{Si}_{29.20}\text{Al}_{6.89}\text{O}_{72}] \cdot 22.9\text{H}_2\text{O}$  with  $E\% = -0.58$  and  $R = 0.86$  (Passaglia and Sheppard, 2001). Although this ferrierite is alkali rich and relatively Mg poor compared with many other ferrierite-Mg compositions, it has too much Mg to be derived in large quantities from the pristine glass. Rice *et al.* (1992) suggested that the source of the Mg in the Lovelock deposit could have originated from a post-depositional brackish lake or from nearby leached basalts. It is important to highlight that, as reported by Rice *et al.* (1992), mordenite also has a fibrous morphology, therefore ferrierite and mordenite could be morphologically indistinguishable under microscopic observation.

## Materials and methods

### Sampling methods

The sampling strategy concerned all the zeolite-rich deposits. The sampling sites were selected taking into account the basic information reported by Rice *et al.* (1992), the *Geologic Map of Nevada* (Crafford, 2007), and the schematic map of Stewart and Carlson (1978). Fig. 1 shows the areal distribution of the sampling points. Samples 1, 1B, 2, 3 and 4 were collected around an open pit in the ferrierite tuffs. Sample 4 was collected in correspondence with an open front of the pit. The raw material is shown in Fig. 2. Samples 5 and 5B are representative of the mordenite-rich tuffaceous sediments present in the eastern part of the study area (Fig. 1). An overview of the Lovelock deposit is shown in Fig. 2. For each sampling point, ~1 kg of rock sample has been collected, stored into polythene bags to avoid inter-contamination and transported to the labs. Before being examined with various analytical techniques, rock samples were prepared by crushing, wet ground (with acetone, to prevent fibres dispersion) and homogenisation/mixing by agate mortar.

### Experimental methods

With the aim to evaluate the nature of the mineral fibres present in the samples, a validated and consolidated protocol of analysis (including morphometric, chemical and mineralogical characterisations) was applied (Gualtieri, 2018; Gualtieri *et al.*, 2018b). The mineral composition of the samples was determined by powder X-ray diffraction (PXRD). The evolution of the release of volatiles from the samples was analysed by thermogravimetric and differential thermal analysis (TG-DTA). Semi-quantitative observations of mineral fibres were performed by scanning electron microscopy (SEM) and transmission electron microscopy (TEM). The geometry of fibrous ferrierite particles ( $L$ ,  $D$  and  $L/D$ ) was determined by digital image processing of the SEM raster graphics. Qualitative elemental analysis of the fibres was accomplished using an X-ray energy-dispersive spectrometer (X-EDS).

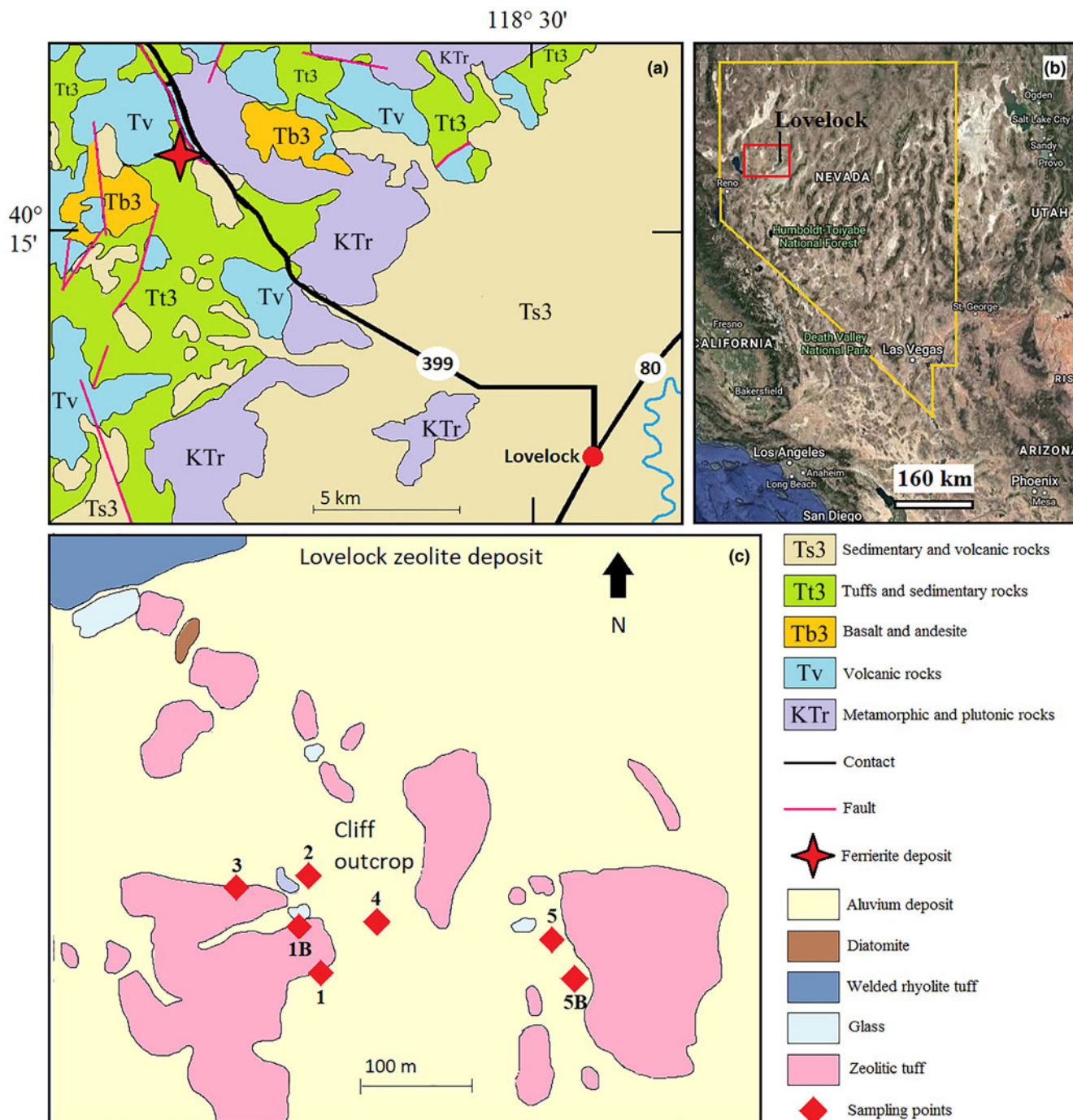
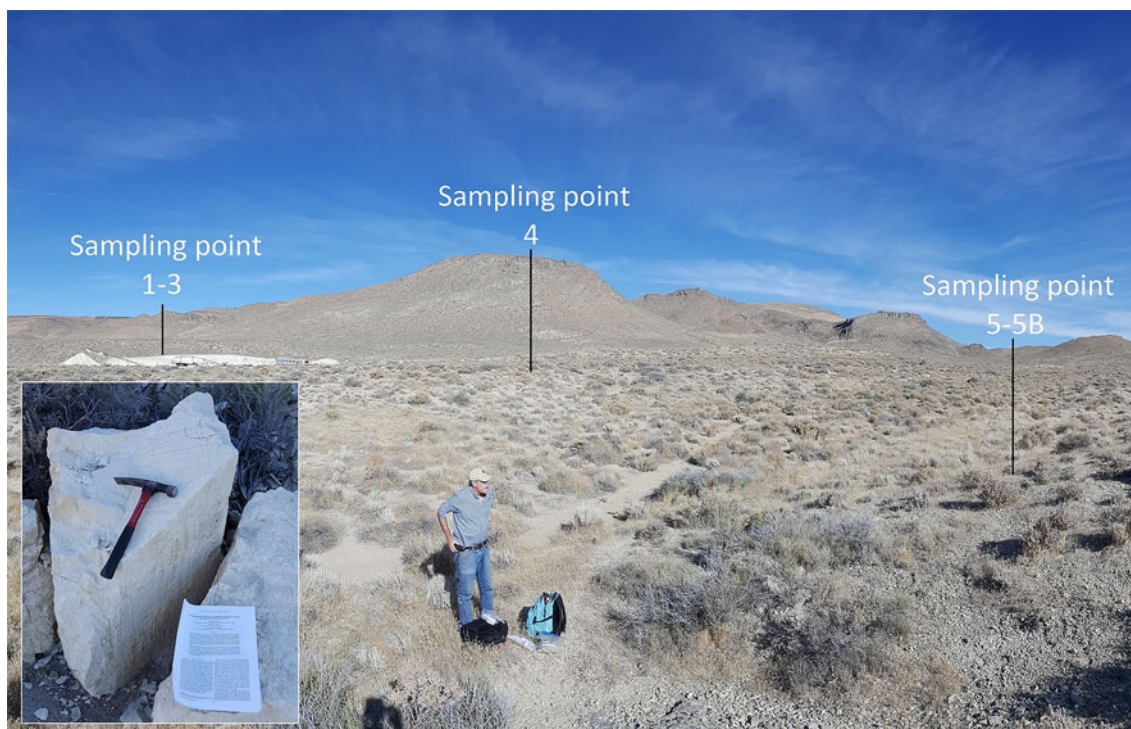


Fig. 1. (a) Geological map of the Lovelock zeolite deposit (modified from Rice *et al.*, 1992); (b) view of Nevada from a Google Earth™ satellite image; the red square identifies the study area; and (c) sampling points.

Unequivocal classification of the mineralogical nature of the fibres present in the samples (in order to discriminate between ferrierite and mordenite), was obtained by micro-Raman spectroscopy. In this regard, given the small size of the fibrous ferrierite particles, the standard phase contrast microscopy (PCM) and polarising light microscopy (PLM) protocols, generally used for qualitative asbestos analysis, are not applicable for examining these rock samples.

Besides fibre morphology, a key parameter that determines the toxicity/pathogenicity of a fibre is biopersistence, one component

of which is biodurability. One key factor that affects fibre biodurability is the surface area (Gualtieri, 2018). In particular, the fibre dissolution rate is directly related to the specific surface area (SSA) and is included as a factor in equations describing dissolution kinetics (Fischer *et al.*, 2014, Gualtieri *et al.*, 2018c). A larger surface area determines a higher reactivity of the mineral fibres in solution. In an acidic environment (such as found in lung tissue) particles with large surface areas (e.g. chrysotile fibres) react more than those with low SSA (e.g. amphibole fibres) (Gualtieri *et al.*, 2018c).



**Fig. 2.** Overview of the site with the location of the sampling spots and an example of the zeolite-rich rock (sample 4) studied in this work.

### Powder X-ray diffraction

Powder X-ray diffraction patterns were collected using a conventional Bragg-Brentano Philips diffractometer (model PW-1729), with  $\theta$ - $2\theta$  geometry,  $\text{CuK}\alpha$  radiation, 40 kV, 30 mA and a KSA Energy dispersive detector. Powders were loaded on an aluminium sample-holder. Data were collected in continuous mode with a 2 mm fixed divergence and antiscatter slits mounted in the incident beam. An integrated step-scan of the detector of  $0.02^\circ 2\theta$  was used with a time of 1 step/s from  $3$  to  $70^\circ 2\theta$ . The qualitative analysis was performed with the *X-Pert High Score Plus* software (Degen *et al.*, 2014) using the ICDD PDF 2 reference database for mineral phases (powder diffraction files from the International Centre for Diffraction Data, <http://www.icdd.com/>).

### Scanning electron microscopy

Scanning electron microscopy analyses were performed using a FEI Nova NanoSEM 450 Field Emission Gun (FEG) SEM equipped with an X-EDS Bruker QUANTAX-200 system, with 20 kV accelerating voltage and  $3.5 \mu\text{A}$  beam current. Small amounts of powder from samples were mixed with 1 mL of acetone. A drop of the suspension was laid on a carbon tape mounted on an Al stub and gold coated (10 nm thick). Images were collected using the signal of both back-scattered and secondary electrons. The surface of the samples was investigated, working at different magnification levels, from  $\times 1000$  up to  $\times 20,000$ . The fibre size and morphometric parameters were determined on  $\sim 100$  individual fibres, using 15 SEM images. Lengths and diameters were calculated using *ImageJ* image analysis software, version 1.52a (NIMH, 2018).

### Micro-Raman Spectroscopy

Raman spectra were obtained using a confocal Jobin Yvon Labram Raman Microscope equipped with a  $1024 \times 256 \times 16$  CCD detector (Peltier cooled), employing a green laser, using a wavelength of 532 nm, pinhole of  $500 \mu\text{m}$ , slit of  $300 \mu\text{m}$  and high-resolution grating of 1800 g/mm. The spectra were collected on single fibres embedded in the sample matrix. The laser was focused with a  $\times 100$  objective (BX-40 Olympus Microscope). Spectra were recorded without any preparation of the samples; the latter simply being laid on a metal support. After focusing on a crystal through a microscope and a CCD camera, the spectrum was recorded with a variable number of scans or an accumulation time according to the intrinsic signal intensity. Collected spectra were processed using *CrystalSleuth* software by Ruff (Laetsch and Downs, 2006).

### Transmission electron microscopy

Transmission electron microscopy investigations were performed using a TEM/STEM FEI Tecnai G2 200 kV instrument, available at the Friedrich-Schiller University of Jena. The original sample, fully described in Gualtieri *et al.* (2018a) was ground gently in an agate mortar with ethanol and then a droplet of suspension was deposited on a Cu TEM grid with a carbon network as support film.

### Determination of the specific surface area (SSA)

The SSA of the sample was determined using the BET-method (Brunauer *et al.*, 1938). The external surface area was determined with the t-plot method (Pollastri *et al.*, 2014). The SSA analyses were measured using a Gemini V instrument (Micromeritics). About 300 mg of dehydrated sample (at 673.15 K for 24 h) was

mounted in the sample holder and conditioned at 323.15 K prior to the measurement. The analysis was carried out using N<sub>2</sub> at the temperature of 77.15 K. Measurements were conducted with an equilibration time of 10 s and the saturation pressure of 777.280 mm Hg.

### Thermogravimetric and differential thermal analysis

Thermogravimetric and differential thermal analysis (TG and DTA) measurements were performed with a Seiko SSC 5200 thermal analyser. To provide a better comparison of the TG/DTA data with those reported in Gualtieri *et al.* (2018a) the same experimental conditions were applied: heating rate, 10°C/min; heating range, 298–1400 K; data measurement, every 0.5 s; DTA reference,  $\alpha$ -alumina powder; purging gas, air at a flow rate of 2  $\mu$ L/min.

### Results

The PXRD patterns are reported in Fig. 3. In all samples, zeolites are the main mineral phases. Samples 1 and 1B are composed only of ferrierite and mordenite, while samples 2, 3, 4, 5 and 5B have orthoclase, clinoptilolite and cristobalite as secondary phases. Using the integrated intensities of the characteristic ferrierite diffraction peaks, a comparison of the content of this zeolite in the samples investigated was performed. Sample 2 has the highest content of ferrierite, while sample 5 has the lowest. Sample 5B does not contain ferrierite. The other samples (2, 3 and 4) have intermediate ferrierite contents between samples 2 and 5. In the sample 5B the main zeolite component is mordenite.

Scanning electron microscopy and TEM/STEM investigations showed a remarkable variation in the presence of fibre particles among the samples (Figs 4 and 5). Sample 2 displays a high concentration of fibre aggregates and bundles ( $L=20\text{--}30\ \mu\text{m}$ ;  $D=5\text{--}10\ \mu\text{m}$ ) which split longitudinally into thinner fibrils (Fig. 4a,b). Instead, in the samples 1, 1B, 3 and 4, fibres are present in minor concentrations and well dispersed into the matrix (Fig. 4c,d). The lowest concentration of fibres was found in the 5 and 5B samples. Fibres appear with a needle-like crystal habit (Fig. 5) although some fibrous crystals have a slight degree of curvature (Fig. 4d, see the dashed line indicating curved fibres). The crystal habit composed of single needles is similar to that of fibrous erionite and different from that usually shown by chrysotile asbestos (flexible bundles of fibres). The analysis of the high-magnification SEM images showed that fibres have a length between 1.8–19.0  $\mu\text{m}$  (average 8.6  $\mu\text{m}$ ) and diameters between 0.1–0.6  $\mu\text{m}$  (average 0.3  $\mu\text{m}$ ), (Table 1). All of the observed fibres have length/width ratio  $>14$  (average 35.4).

Energy-dispersive spectroscopy (EDS) microanalyses of some fibre bundles, showed the presence of two main chemical compositions indicative of ferrierite and mordenite (Fig. 6 and supplementary material). Ferrierite, as reported in the literature (Wise and Tschernich, 1976, Rice *et al.*, 1992) can be recognised by the presence of Mg in the EDS spectrum. In addition, as previously shown by Rice *et al.* (1992), the Lovelock ferrierite has distinctively high K concentrations. Mordenite fibres are easily distinguishable from ferrierite by the lack of Mg in their chemical composition (Fig. 6). However, as fibrous ferrierite is associated intimately with other mineral phases (often orthoclase), it was not possible to determine if the trace elements identified in the EDS spectra (such as Mg and K) were related to the fibres or the other phases present in the samples. For this purpose,

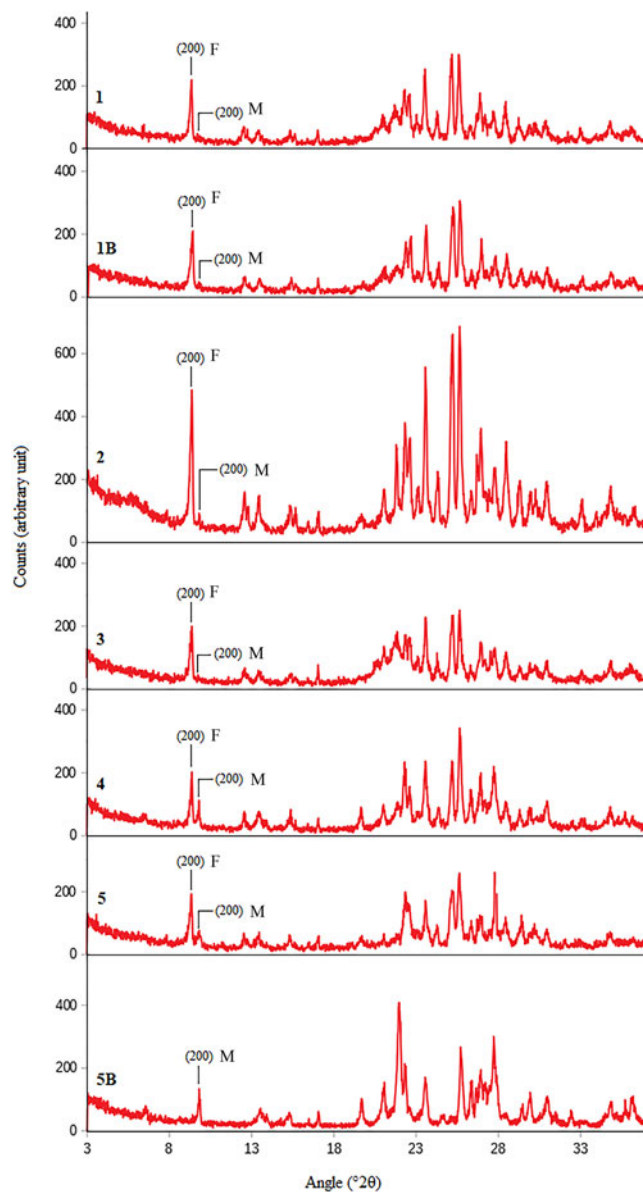
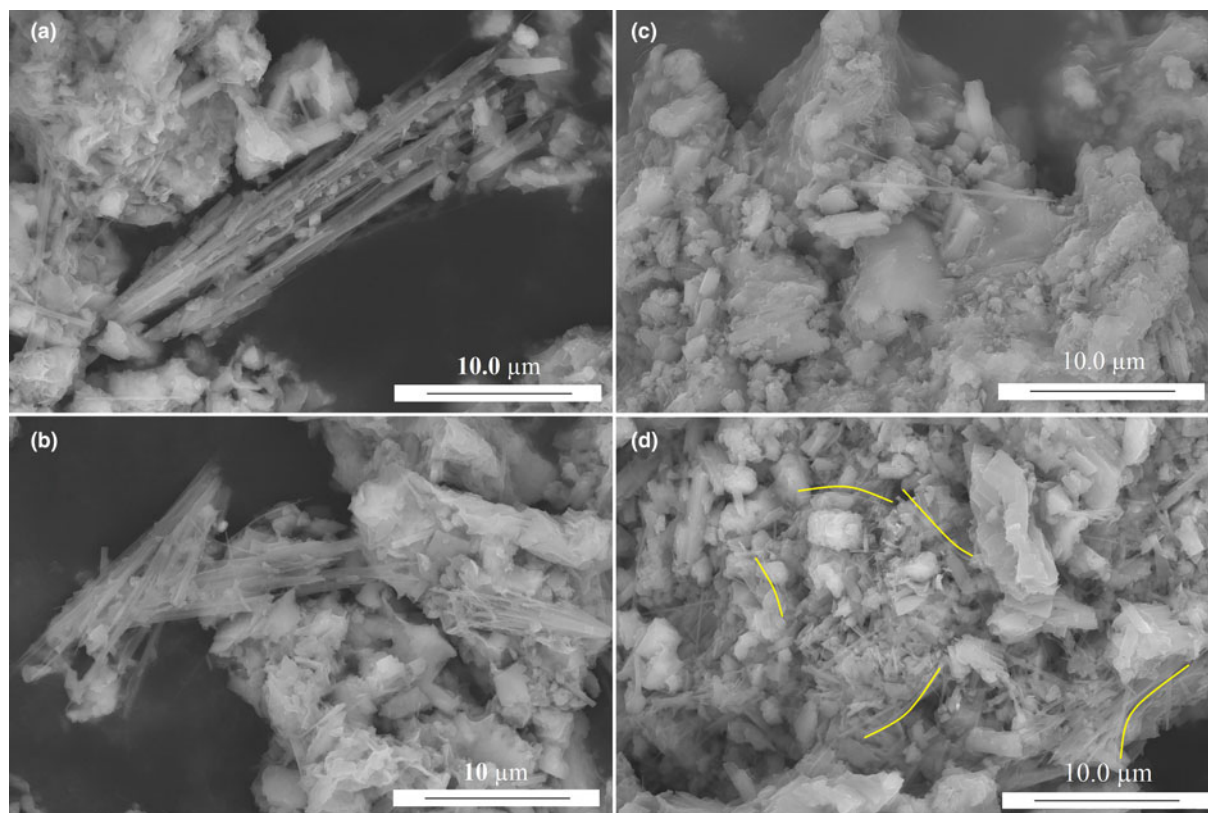
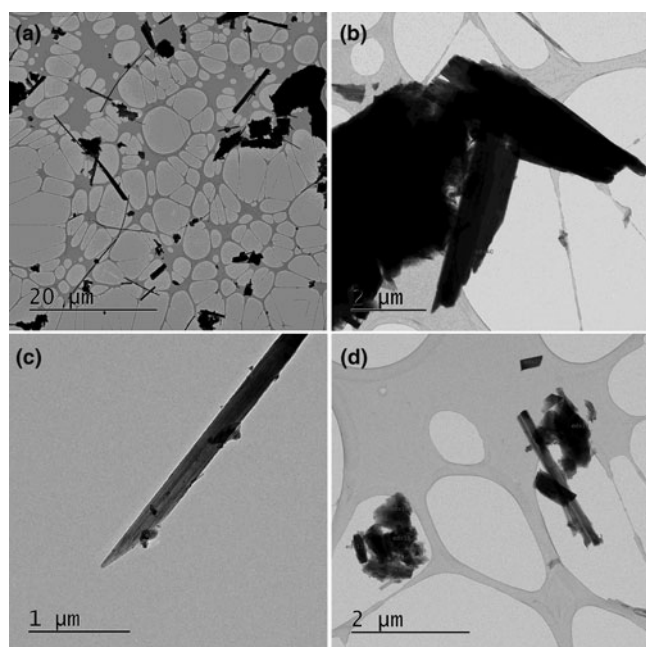


Fig. 3. Selected region of the collected diffraction patterns. The peaks of ferrierite (F) and mordenite (M) are labelled with their Miller's indices, in both cases the (200).

identification of the mineralogical nature of the fibres was made using micro-Raman spectroscopy. Micro-Raman spectra of selected fibres are reported in Fig. 7. For reference the spectrum of pure ferrierite (BC) from Monte Lake, British Columbia, Canada, is also shown in Fig. 7a. The most intense intra-tetrahedral band at 431  $\text{cm}^{-1}$  is sensitive to the T–O–T angle (Dutta and Del Barco, 1988). The other major bands (Lercher and Jentys, 2007, Gualtieri *et al.*, 2018a) are at 330  $\text{cm}^{-1}$  (pore opening inter-tetrahedral mode), 543  $\text{cm}^{-1}$  (double ring inter-tetrahedral) and 780  $\text{cm}^{-1}$  (inter-tetrahedral symmetric stretching). Spectra reported in Fig. 7b and Fig. 7c are representative of fibres found in samples 2 and 3, respectively. The diagnostic bands of ferrierite (see BC samples, Fig. 7a) are present. Figure 8d shows the Raman spectrum of a mordenite fibre found in sample 5. In all acquired spectra, the typical bands of orthoclase are invariably observed.



**Fig. 4.** FEG-SEM microphotographs of the fibres: (a,b) fibres bundles inside sample 2; (c) single fibre in sample 3; (d) fibrous cluster embedded in the matrix from sample 5. Some fibres have a curved and flexible shape.



**Fig. 5.** TEM microphotographs of the fibres: (a) low magnification overview; (b) fibrous aggregates of ferrierite in sample 2; (c) needle-like mordenite fibres from sample 4; and (d) ferrierite and mordenite fibres partially embedded by the matrix in sample 3.

**Table 1.** Results of the SEM dimensional analysis of fibres\*.

	Min	Max	Average	25th percentile	75th percentile
$L$ ( $\mu\text{m}$ )	1.8	19.0	8.6	5.7	10.8
$D$ ( $\mu\text{m}$ )	0.1	0.6	0.3	0.2	0.3
$L/D$	14.6	78.0	35.4	23.8	40.9

\*Legend:  $L$  (length);  $D$  (width);  $L/D$  (aspect ratio)

High-resolution TEM investigations showed that fibrous ferrierite tends to occur as bundles and aggregates with mordenite (Fig. 5). Moreover, both fibrous ferrierite and mordenite aggregates are often embedded into a matrix rich in phyllosilicates (Supplementary figure, see below).

The SSA data was measured for sample 2 with the highest ferrierite content and the measured value of the BET surface area of the natural sample was 23(1)  $\text{m}^2/\text{g}$ .

Thermal analyses for samples 2 and 3 (Fig. 8) show that in both samples, three main endothermic events occur with maximum reaction rates at about 336, 441 and 700 K.

The first reaction (maximum rate at 336 K), even if it is better resolved in sample 3, drives to similar weight loss (4.23 and 4.17% in samples 2 and 3, respectively, calculated in the thermal range 273–395 K). On the other hand, the second reaction (maximum rate at 441 K and occurring between 395 and 650 K) is less resolved and more relevant in sample 2 (weight loss 4.29%)

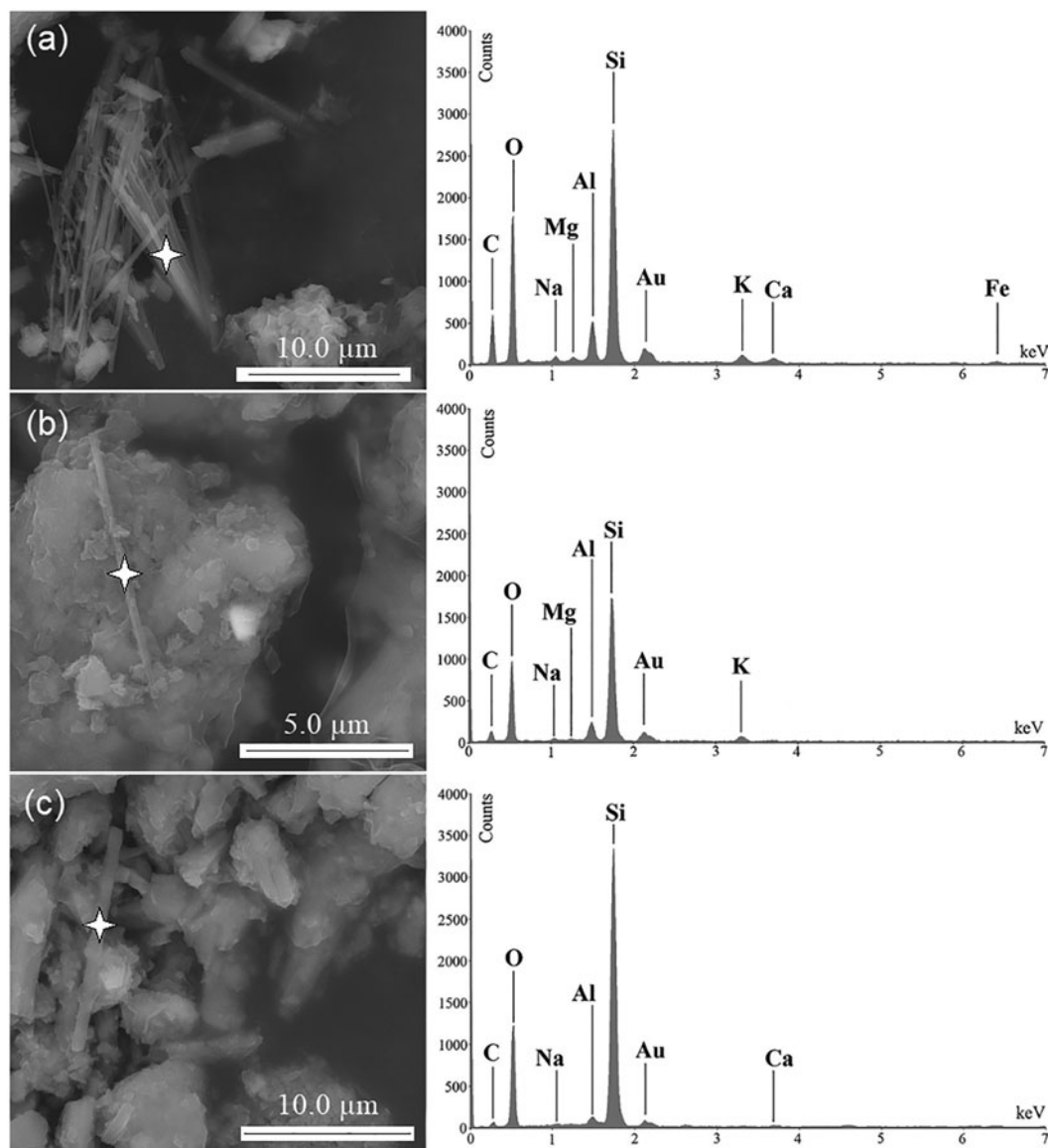


**Fig. 6.** FEG-SEM microphotographs of the fibres and EDS micro-analyses of selected fibres: (a) bundles of fibrous ferrierite in sample 2; (b,c) ferrierite and mordenite fibres respectively, from sample 5.

than in sample 3 (weight loss 3.31%). The third reaction occurs between 650 and 950 K and the weight loss is 0.82 and 0.64% for sample 2 and 3, respectively. Thermal events at temperatures higher than 1000 K, shown by the DTA curves, are related to recrystallisation and/or partial melting.

The thermal events observed between 273 and 950 K are related to the release of water that, as typical in ferrierite, begins from the very early heating stages (Arletti *et al.*, 2018). The total amount of structural water for samples 2 and 3 is 9.34% and 8.12%, respectively.

## Discussion

This work is focussed on the mineralogical and morphometric characterisation of rhyolitic tuffs at Lovelock, Nevada with special attention to the fibrous zeolites ferrierite and mordenite. The multi-analytical methods applied in this study confirm the occurrence of fibrous ferrierite in the rhyolitic tuffs at Lovelock, Nevada

is not a mineral rarity. The major concentration of fibrous ferrierite was found in the tuff deposits in correspondence with a small open pit mining operation (south-west study area). The fibrous ferrierite content decreases in the sedimentary deposits at the base of the ferrierite rich tuffs, while it is not present in the pyroclastic depositions located in the south-east area where mordenite is the main zeolite product. In contrast to the results from Rice *et al.* (1992), we found no evidence that mordenite is the major zeolite phase in the superficial levels of the Lovelock deposit. This discrepancy is probably due to the difference in the sampling methodology: in our work, a surface sample collection was obtained, whereas the study by Rice *et al.* (1992) was based on the investigation of four cores with poor lateral correlation.

Transmission electron microscopy investigations showed an intimate intermix of the fibrous zeolites with layer silicates, whereas SEM and micro-Raman results displayed a dense intergrowth between ferrierite and K-feldspar. These outcomes are in agreement with the paragenesis described by Rice *et al.*

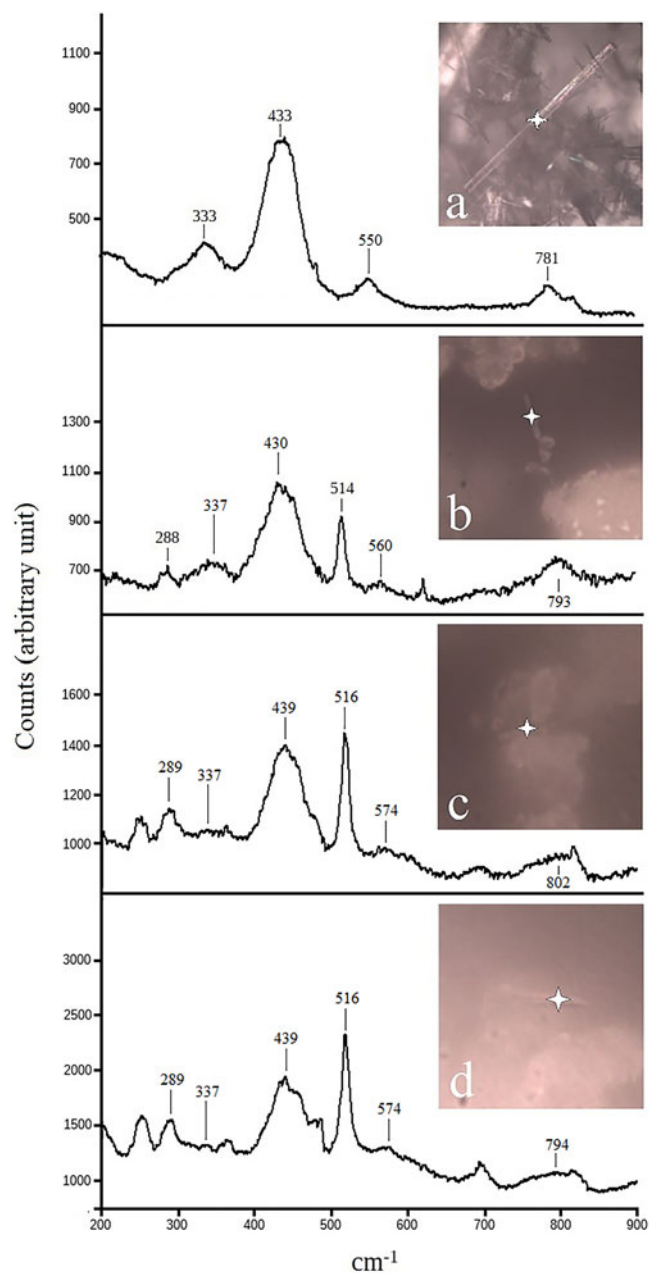


**Fig. 7.** Micro-Raman spectra of selected fibres: (a) standard BC ferrierite; (b) a ferrierite fibre from sample 2; (c) a ferrierite fibre from sample 1; (d) spectrum of a fibre from sample 5, a mixture between ferrierite and mordenite, the latter giving a double band in the range 400–500  $\text{cm}^{-1}$ . Note that all the samples show the orthoclase peak around 510  $\text{cm}^{-1}$ .

(1992) who hypothesised an initial crystallisation of smectite followed by an almost contemporary co-crystallisation of ferrierite, orthoclase and, appreciably later, of mordenite. Thermal analyses are in agreement with PXRD results with sample 2 showing the highest zeolitic content among the samples investigated.

In the Lovelock rock samples, fibrous ferrierite and fibrous mordenite are mostly intermixed and only careful EDS micro-analysis and micro-Raman investigations enabled us to identify and distinguish them. The crystal habit of both the two zeolites is fibrous. Fibres are thin ( $<0.6 \mu\text{m}$ ), sometimes slightly flexible and often aggregated in bundles (asbestiform habit). Samples taken in the mining area contain fibrous ferrierite fibres that are

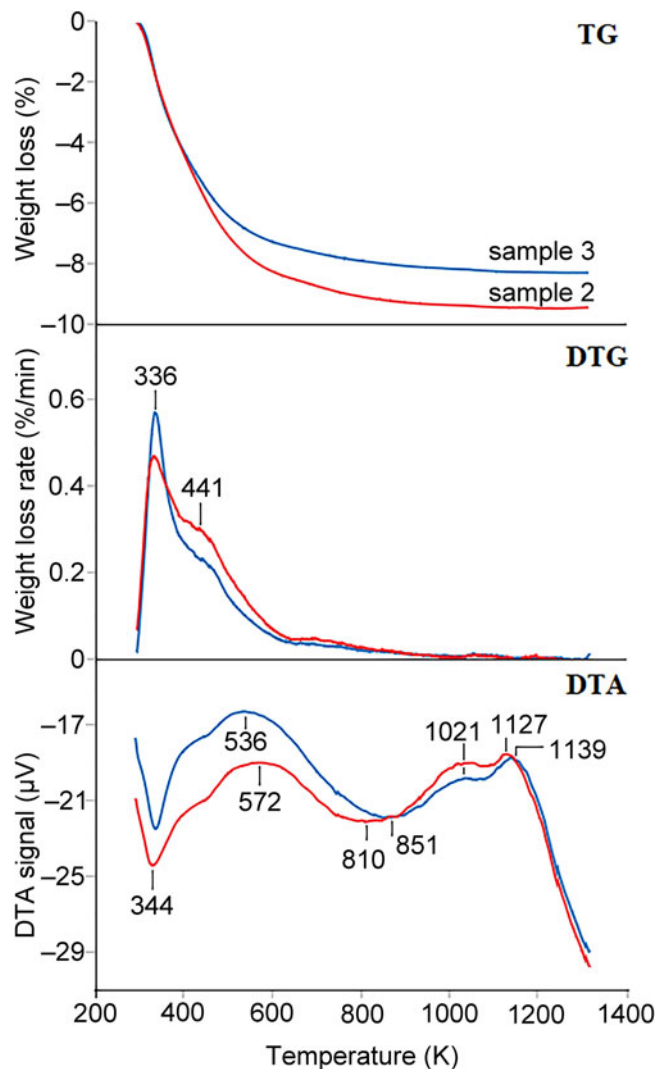


**Fig. 8.** Comparison between the TG, the TG first derivative (DTG), and DTA curves of sample 2 (red line) and sample 3 (blue lines). In the DTA curve, a minimum represents an endothermic reaction.

classified as breathable (regulated) according to the WHO (1997) counting criteria (particles with  $L \geq 5 \mu\text{m}$ ,  $D \leq 3 \mu\text{m}$ ,  $L/D$  ratio  $\geq 3:1$ ). Because Gualtieri *et al.* (2018a) showed that fibrous ferrierite displays features similar to the positive carcinogenic standard fibrous erionite-Na from Jersey, Nevada, the widespread occurrence of this mineral fibre in the Lovelock area must be considered as a possible source of an environmental exposure hazard. Potential public exposure to breathable mineral dust from natural deposits in which asbestos-like fibres can be hosted is an issue of great concern in the USA, and other part of world (Battles and Barton, 1995; Johnson *et al.*, 1993; Carten, 1986; Gualtieri *et al.*, 2018b; Lucci *et al.*, 2018). These deposits are commonly referred to as naturally occurring asbestos, NOA (Lee *et al.*, 2008; Harper, 2008). In the USA, the Agency for Toxic Substances and Disease Registry has recently released a map showing considerable overlap between the 100 fastest growing counties in the United States and known areas of NOA (Lee *et al.*, 2008).

Although the occurrence of fibrous ferrierite concerns a desert-like area with minor presence of any potentially exposed



population, the presence of an open pit could be a source of concern. For this reason, it is recommended to adopt a precautionary approach for possible mining operations in that area to prevent or minimise the risk of exposure while waiting for *in vitro* and *in vivo* tests that should ultimately assess the toxicity/pathogenicity potential of fibrous ferrierite. A precautionary approach is recommended whenever risk of hazardous mineral exposure for the population is deemed to be high. The application of the precautionary approach is justified when situations similar to the erionite Cappadocian case, where fibrous erionite found in the bedrock of three villages in central Anatolia, Turkey, caused a high-level environmental exposure to the villagers, leading to massive numbers of malignant pleural mesothelioma cases (see for example, Metintas *et al.*, 1999).

## Conclusions

In this study, a multidisciplinary approach, based upon extensive sample collection, mineralogical characterisation, morphometric observations and chemical analysis, was applied to assess the occurrence and content of fibrous ferrierite in the rhyolitic tuffs at Lovelock, Nevada. The results confirm that fibrous ferrierite is widespread in the deposit and is often intermixed with fibrous mordenite. The crystal habit of the two zeolite species is similar with a fibrous-asbestiform character: thin ( $D < 0.6 \mu\text{m}$ ), elongated (average  $L = 8.6 \mu\text{m}$ ) slightly flexible and aggregated in bundles. As noted in the investigation of similar minerals from Yucca Mountain, Nevada, USA (Stephenson *et al.*, 1999) these minerals are likely to be respirable when aerosolised.

The overall mineralogical compositions are in agreement with those reported by Rice *et al.* (1992), although a different spatial distribution of the zeolite phases was found. Ferrierite and mordenite are the major mineralogical components in the rock samples studied (clinoptilolite, orthoclase and cristobalite are secondary phases), however ferrierite is predominant in the tuff deposits at south-west area of the study area (sample 2), whereas its content decreases in the sedimentary deposits at the base of the tuffs outcrops (samples 3 and 4) and it is not present in the mordenite-rich tuff in the south-west area (sample 5B).

As fibrous ferrierite is associated intimately with mineral phases that interfere with analysis (mordenite and orthoclase), the identification of the mineralogical nature of the fibres was only possible through the use of micro-Raman spectroscopy. The greatest concentration of fibrous ferrierite was found in the ferrierite tuff deposits (south-west area) in correspondence with a small open pit. Because Lovelock's fibrous ferrierite is composed mostly of fibres covered by WHO (1997) regulations, with morphological and chemical-physical properties close to that of the carcinogenic fibrous erionite, any process involving the handling of rocks of this deposit should be carefully monitored in order to reduce the risk of exposure.

The present results, together with the previous outcome of Gualtieri *et al.* (2018a), strongly suggest the need for detailed identification and mapping of natural sites characterised by the potential occurrence of fibrous minerals, with particular regard to unclassified fibres like ferrierite. In this context, the procedure proposed in this study may be a suitable tool to identify the mineralogical nature of fibrous minerals in outcrops (or raw materials) and assess if they may represent a potential health hazard.

**Acknowledgements.** We thank K. Pollok and N. Bursi for the TEM data collected at the Friedrich-Schiller University of Jena (Germany). This research

was funded by the Italian grant "Fondi di Ateneo per la Ricerca" (FAR 2017) "Fibre potential toxicity Index (FPTI). A quantitative model to evaluate the toxicity and pathogenicity of mineral fibres, including asbestos". We thank the two competent referees for their careful revision that certainly improved the quality of the final version of the paper.

**Supplementary material.** To view supplementary material for this article, please visit <https://doi.org/10.1180/mgm.2019.25>.

## References

- Arletti R., Fantini R., Giacobbe C., Gieré R., Vezzalini G., Vigliaturo R. and Quartieri S. (2018) High-temperature behavior of natural ferrierite: In-situ synchrotron X-ray powder diffraction study. *American Mineralogist*, **103**, 1741–1748.
- Battles D.A. and Barton M.D. (1995) Arc-related sodic hydrothermal alteration in the western United States. *Geology*, **23**, 913–916.
- Brunauer S., Emmet P.H. and Teller E. (1938) Adsorption of gases in multimolecular layers. *Journal of the American Chemical Society*, **60**, 309–319.
- Carbone M., Emri S., Dogan A.U., Steele I., Tuncer M., Pass H.I. and Baris Y.I. (2007) A mesothelioma epidemic in Cappadocia: Scientific developments and unexpected social outcomes. *Nature Reviews Cancer*, **7**, 147–154.
- Carten R.B. (1986) Sodium-calcium metasomatism, chemical, temporal, and spatial relationships at the Yerington, Nevada; porphyry copper deposit. *Economic Geology*, **81**, 1495–1519.
- Crafford A.E.J. (2007) *Geologic Map of Nevada*. U.S. Geological Survey, Data Series, 249.
- Degen T., Sadki M., Bron E., König U. and Nénert G. (2014) The HighScore Suite. *Powder Diffraction*, **29**, 13–18.
- Dutta P.K. and Del Barco B. (1988) Raman spectroscopy of zeolite A: influence of silicon/aluminum ratio. *The Journal of Physical Chemistry*, **92**, 354–357.
- Fischer C., Kurganskaya I., Schäfer T. and Lüttge A. (2014) Variability of crystal surface reactivity: what do we know? *Applied Geochemistry*, **43**, 132–157.
- Gottardi G. and Galli E. (1985) *Natural Zeolites*. Springer, Berlin, 409 pp.
- Graham R.P.D. (1918) On ferrierite, a new zeolitic mineral, from British Columbia. *Royal Society of Canada, Proceedings and Transactions*, **3rd Series**, **12**, 185–190.
- Gramlich-Meier R., Meier W.M. and Smith B.K. (1984) On faults in the framework structure of the zeolite ferrierite. *Zeitschrift für Kristallographie – Crystalline Materials*, **169**, 201–210.
- Gramlich-Meier R., Gramlich V. and Meier W.M. (1985) The crystal structure of the monoclinic variety of ferrierite. *American Mineralogist*, **70**, 619–623.
- Gualtieri A.F. (2018) Towards a quantitative model to predict the toxicity/pathogenicity potential of mineral fibers. *Toxicology Applied Pharmacology*, **361**, 89–98.
- Gualtieri A.F., Bursi Gandolfi N., Passaglia E., Pollastri S., Mattioli M., Giordani M., Ottaviani M.F., Cangiotti M., Bloise A., Barca D., *et al.* (2018a) Is fibrous ferrierite a potential health hazard? Characterization and comparison with fibrous ferrierite. *American Mineralogist*, **103**, 1044–1055.
- Gualtieri A.F., Bursi Gandolfi N., Pollastri S., Rinaldi R., Sala O., Martinelli G., Bacci T., Paoli F., Viani A. and Vigliaturo R. (2018b) Assessment of the potential hazard represented by natural raw materials containing mineral fibres – The case of the feldspar from Orani, Sardinia (Italy). *Journal of Hazardous Materials*, **350**, 76–87.
- Gualtieri A.F., Pollastri S., Bursi Gandolfi N. and Lassinantti Gualtieri M. (2018c) *In vitro* acellular dissolution of mineral fibres: A comparative study. *Scientific Reports*, **8**, 7071.
- Harper M. (2008) 10th Anniversary Critical Review: Naturally occurring asbestos. *Journal of Environmental Monitoring*, **10**, 1394–1408.
- IARC (International Agency for Research on Cancer) (2012) Asbestos (chrysotile, amosite, crocidolite, tremolite, actinolite, and anthophyllite). *IARC Monographs on the Evaluation of the Carcinogenic Risks to Humans*, **100C**, 219–309.
- IARC (International Agency for Research on Cancer) (2017) Some nanomaterials and some fibres. *IARC Monographs on the Evaluation of the Carcinogenic Risks to Humans*, **111**, 215–240.

- Johnson D.A., Barton M.D. and Hassanzadeh J. (1993) Mafic and felsic hosted Fe-apatite-(REE-Cu) mineralization in Nevada. *Abstracts with Programs – Geological Society of America*, **25**, 57.
- Laetsch T. and Downs R. (2006) Software for identification and refinement of cell parameters from powder diffraction data of minerals using the RRUFF Project and American Mineralogist crystal structure databases. Abstracts from the 19th General Meeting of the International Mineralogical Association, Kobe, Japan, 23–28 July 2006.
- Lee R.J., Strohmeier B.R., Bunker K.L. and Van Orden D.R. (2008) Naturally occurring asbestos: A recurring public policy challenge. *Journal of Hazardous Material*, **153**, 1–21.
- Lercher J.A. and Jentys A. (2007) Infrared and Raman spectroscopy for characterizing zeolites. *Studies in Surface Science and Catalysis*, **168**, 435–476.
- Lucci F., Della Ventura G., Conte A., Nazzari M. and Scarlato P. (2018) Naturally occurring asbestos (NOA) in granitoid rocks, a case study from Sardinia (Italy). *Minerals*, **8**, 442.
- Metintas M., Hillerdal G. and Metintas S. (1999) Malignant mesothelioma due to environmental exposure to erionite: follow-up of a Turkish emigrant cohort. *European Respiratory Journal*, **13**, 523–526.
- NIMH (National Institute of Mental Health) (2018) *ImageJ*. <https://imagej.nih.gov/ij/> (Accessed 19, September 2018).
- Passaglia E. and Sheppard R.A. (2001) The crystal chemistry of zeolites. Pp. 69–116 in: *Natural Zeolites: Occurrence, Properties, Applications* (D. Bish and D. Ming, editors). Reviews in Mineralogy and Geochemistry, **45**. Mineralogical Society of America and Geochemical Society, Washington DC.
- Pollastri S., Gualtieri A.F., Gualtieri M.L., Hanuskova M., Cavallo A. and Gaudino G. (2014) The zeta potential of mineral fibres. *Journal of Hazardous Materials*, **276**, 469–479.
- Rice S.B., Papke K.G. and Vaughan D.E.W. (1992) Chemical controls on ferrierite crystallization during diagenesis of silicic pyroclastic rocks near Lovelock, Nevada. *American Mineralogist*, **77**, 314–328.
- Stewart J.H. and Carlson J.E. (1978) *Geologic Map of Nevada*. U.S. Geological Survey.
- Stephenson D.J., Fairchild C.I., Buchan R.M. and Dakins M.E. (1999) A fiber characterization of the natural zeolite, mordenite: A potential inhalation health hazard. *Aerosol Science & Technology*, **30**, 467–476.
- Vaughan P.A. (1966) The crystal structure of the zeolite ferrierite. *Acta Crystallographica*, **21**, 983–990.
- WHO (World Health Organization) (1997). *Determination of Airborne Fiber Number Concentrations*. World Health Organization, Geneva, pp. 53.
- Wise W.S. and Tschermich R.W. (1976) Chemical composition of ferrierite. *American Mineralogist*, **61**, 60–66.